Two Mechanisms Determine Quantum Dot Blinking

Gangcheng Yuan[1], Daniel E. Gomez[2], Nicholas Kirkwood[1,3], Klaus Boldt[1,4], and Paul Mulvaney[1]*

1 School of Chemistry and Bio21 Institute, University of Melbourne, Parkville, Victoria 3010, Australia
2 RMIT University, Melbourne, Victoria, 3000, Australia.

3 Current Address: Opto-Electronic Materials Section, Faculty of Applied Sciences, Delft University of Technology, Van der Maasweg 9, 2629HZ Delft, The Netherlands
4 Current Address:Department of Chemistry and Zukunftskolleg, University of Konstanz, 78457 Konstanz, Germany
** e-mail: mulvaney@unimelb.edu.au*

Abstract

Many potential applications of quantum dots (QDs) can only be realized once the luminescence from single nanocrystals is understood. These applications include the development of quantum logic devices, single photon sources, long-life LEDs, and single molecule biolabels. At the single nanocrystal level, random fluctuations in the QD photo-luminescence (PL) occur, a phenomenon termed blinking. There are two competing models to explain this blinking: Auger recombination and surface trap induced recombination. Here we use lifetime scaling on core-shell NCs with close to unity quantum yield to demonstrate that both types of blinking occur in the same QDs. We prove that Auger-blinking can yield exponential on/off times in contrast to earlier work. The surface passivation strategy determines which blinking mechanism dominates. This study unifies earlier studies on blinking mechanisms and provides direct evidence that stable single QDs can be engineered for optoelectronic applications.

Quantum dots (QDs) are beginning to appear in modern electronic devices such as light-emitting diodes[1] and single-photon sources,[2] but their performance is limited by blinking, a photoluminescence (PL) fluctuation between bright (*on*) and dark (*off*) states.[3, 4] A charging model[5] was first proposed to explain blinking. In this model, the PL fluctuation is due to photoionization[6] and neutralization. In a neutral QD, *on* state emission is produced *via* radiative recombination. Once the QD is photoionized, fast Auger recombination quenches the emission *via* transfer of the exciton energy to the third carrier in the core. However, while the charging model predicts an exponential distribution of both the *on* and *off* durations, they are found to be power-law distributed from experiment.[7] Modified charging models have been presented to explain the origin of power-law blinking, typically by varying the barriers into and out of multiple traps or by energetic diffusion.[8-11] We will denote this type of behavior "Auger-blinking".

Over the past ten years, it has been realized that the simple charging model is not sufficient to explain the origin of the *off* state.[12, 13] The Auger quenching rate of singly charged exciton (trion)[14] does not explain the low quantum yield (QY) of the *off* state,[12, 15, 16] unless multiply charged excitons are invoked; alternatively, it is possible that charging may not be the only reason for the *off* state. It has also been reported that there exist continuous emission states with varying non-radiative rates but fixed radiative rates,[17-20] this behavior is referred to here as "BC-blinking" because as we show later, such blinking is from bandedge carrier trapping. Such observations are consistent with a model without the long-lived traps[21] and also with a later model using multiple recombination centers (MRC model).[22] In the MRC model, multiple emission states arise due to a set of non-radiative recombination centers which are switching between activation and deactivation, and no charging is required.

With progress in QD synthesis and measurement, further blinking-related behaviors have been identified.[23-29] Blinking can be suppressed by passivating the traps or suppressing Auger recombination,[30] and even non-blinking QDs have been realized.[31-35] Despite empirical progress on the control of blinking, its exact mechanism is still under debate.[4, 36-38] In addition to the Auger-blinking, a new type of blinking due to interception of hot carriers ("HC-blinking"), has been reported, which is distinct from BC-blinking.[29] Since neither the charging model nor the MRC model excludes the other, a combination of both blinking models has also been tried.[39] But experiments on a combination of Auger- and BC- blinking are still lacking.

Here, we report unequivocal evidence that both types of blinking occur in the same QDs, thus unifying previous experiments and models. Emissive states with reduced QYs but equal radiative decay rates compared to the bright states are observed. These grey states cannot be explained by the charging model. On the contrary, they provide direct evidence that blinking can be initiated *via* opening and closing of non-radiative recombination centers. We compare the radiative lifetime scaling, examine correlations in QD lifetime and analyse the PL intensity fluctuations for QDs exhibiting both BC-blinking and Auger-blinking. We show that almost all blinking behaviors in quantum dots can be understood via one of these two models. We do not include HC-blinking in the analysis because it was not observed in our systems.

Results

A. BC-blinking

One of the reasons for blinking is opening and closing of non-radiative channels (Figure 1a). Such channels can be created by fluctuations in adsorbate binding to the semiconductor crystal

surface. This model predicts a linear relationship between PL intensity and lifetime. The intensity I is proportional to the QY, and hence directly proportional to the lifetime τ, and inversely proportional to the radiative lifetime τ_r according to

$$I \propto \mathrm{QY} = \frac{k_r}{k_r + k_{nr}(t)} = \tau k_r = \frac{\tau}{\tau_r} \qquad (1),$$

where k_r is the radiative decay rate and $k_{nr}(t)$ is the non-radiative decay rate that evolves with time. Figure 1b shows a typical trace of the PL intensity as a function of time collected from a single QD (QD 1, QD@639nm, graded shell CdSe/$Cd_xZn_{1-x}S$ QDs[40], see Methods). The PL jumps among a set of intensity levels. The linear correlation of the PL lifetime and intensity is confirmed by the plot of the fluorescence lifetime-intensity distribution (FLID) in Figure 1d. From the linear FLID pattern, we can infer that the radiative decay rate k_r (or the radiative lifetime τ_r), does not change with time. Therefore, the PL intensity fluctuations in Figure 1b are only due to changes in the non-radiative channels, as depicted in Figure 1a. In many cases blinking was too fast to resolve grey states (our bin width was 20 ms). However, we were able to confirm the unchanged radiative lifetime in a few cases where we observed slow intensity-switching events. Such an analysis is presented in Figure 1. The traces in Figure 1b show two periods with stable PL intensities, corresponding to a bright state (red line) and a grey state (black line), which are selected for the lifetime-intensity analysis below. Within each period, the intensity is stable (I_1=167 counts / 20 ms, I_2= 100 counts / 20 ms, while the background noise is 2 counts / 20 ms), and the PL decays in Figure 1c can be fitted well by single exponential functions (τ_1=23.2 ns, τ_2=14.3ns). The radiative lifetime ratio of the two periods is close to unity as

$$\frac{\tau_{r1}}{\tau_{r2}} = \frac{\tau_1}{\tau_2} \cdot \frac{I_2}{I_1} = \frac{23.2}{14.3} \times \frac{100 - 2(\mathrm{background})}{167 - 2(\mathrm{background})} \approx 0.96\,.$$

From the unity radiative lifetime scaling, we infer that the grey states here are not charged or trion states, because the radiative lifetime scaling between the charged and neutral states is approximately 2,[14] as shown later. Hence, there must be a mechanism other than charging that is responsible for the blinking in Figures 1b-d. Our results are partially consistent with the MRC model. [22] In the MRC model, in addition to the radiative pathway, the exciton can also non-radiatively relax through multiple recombination centers. The opening and closing of each center modulates the non-radiative rate and hence the PL intensity. Although it is challenging to explain why these centers randomly switch on and off,[41, 42] this linear correlation of lifetime and intensity has been observed frequently in different QD systems.[17-19] Interestingly, the BC-blinking here is comparable to the HC-blinking reported previously. Both are related to non-radiative recombination,[29] however, the competition between radiative and non-radiative pathways is different. HC-blinking results from the activation and deactivation of the bypass channel, which may be associated with emptying and filling of the corresponding surface trap states. In HC-blinking events, some hot carriers can be intercepted by surface states before cooling down to the band edge. These carriers do not contribute to the PL intensity because of non-radiative recombination following the interception. But some unintercepted hot excitons can successfully reach the band edge after cooling and contribute to the PL intensity and lifetime in the measurement. In the single-exciton regime, the PL lifetime of band-edge excitons does not change together with light intensity. In the BC-blinking observed here, the competition between the radiative and non-radiative recombination occurs after the cooling of hot excitons. In the non-radiative process, hot excitons first reach the band edge, then the hole (electron) is trapped by the surface traps, and subsequently, it recombines non-radiatively with the core state electron (hole).[13] These traps are short-lived (*e.g.*, shallow traps), and the timescale of trapping

and non-radiative recombination is close to that of radiative recombination of the band-edge exciton. The competition between the fixed radiative and fluctuating non-radiative relaxations leads to the linear correlation between lifetime and intensity.

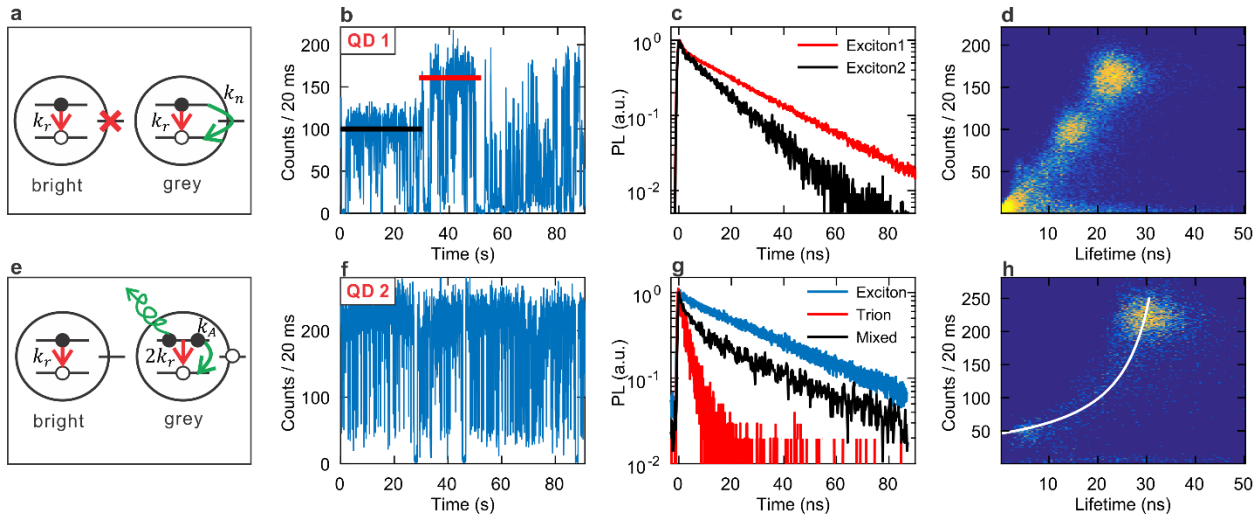

Figure 1 **BC-blinking (top panels) and Auger-blinking (bottom panels).** Two single QDs (QD 1 and QD 2, QD@639nm) were excited at 100 nW. **(a)** BC-blinking. When the trapping channel is blocked, only the radiative rate k_r exists; when the trapping channel is unblocked, the non-radiative rate k_{nr} appears. **(b)** Photoluminescence intensity trace of QD 1. Multiple intensity levels exist including a bright state (exciton1, red line) and a well-defined grey exciton state (exciton2, black line). **(c)** The PL decays of QD 1. The bright state (exciton1, red line) and the grey state (exciton2, black line). **(d)** FLID of QD 1. **(e)** Auger-blinking. In the exciton state, only the radiative rate k_r exists; in the trion state, the non-radiative Auger rate k_A appears, and the radiative rate becomes $2k_r$. **(f)** Photoluminescence intensity trace of QD 2. **(g)** Photoluminescence time decays for the three intensity levels of QD 2. Exciton (220 counts / 20 ms, blue line), trion (50 counts / 20 ms, red line), mixed (110 counts / 20ms, black line). **(h)** FLID of QD 2. The white line is given by Equation (2).

B. Auger-blinking

When the BC-blinking can be suppressed, it is very easy to observe the conventional Auger-blinking, due to exciton-trion transitions (Figure 1e), especially at high excitation powers. The Auger-blinking has features distinct from the BC-blinking. A typical exciton-trion trace

from a single QD (QD 2, QD@639nm) is presented in Figure 1f. Two intensity levels can clearly be seen, corresponding to exciton *X* and trion X^*, respectively (I_X=220 counts / 20 ms, and I_{X^*}=50 counts / 20 ms). As the PL intensity switches mostly between exciton and trion states, the dark state with background noise (5 counts / 20 ms) is ignored in the following analysis. Figure 2g shows the mono-exponential PL decays for the exciton and trion states. After single exponential function fitting, exciton lifetime τ_X, and trion lifetime τ_{X^*} are estimated to be 29.6 ns and 3.1 ns, respectively. The ratio of the two radiative lifetimes,τ_{Xr} and τ_{X^*r}, is

$$\frac{\tau_{Xr}}{\tau_{X^*r}} = \frac{\tau_X}{\tau_{X^*}} \cdot \frac{I_{X^*}}{I_X} = \frac{29.6}{3.1} \times \frac{50-5}{220-5} \approx 2.00\,.$$

For radiative recombination of excitons, one electron recombines with one hole; for trion radiative recombination, both two electrons (holes) have a chance to recombine with one hole (electron). The scaling order, 2, is a useful signature of exciton-trion blinking.[14] Figure 1g also presents the PL decay of an arbitrarily selected intermediate state (110 counts / 20 ms) between exciton and trion states. The bi-exponential PL decay of this intermediate state can be fitted with a combination of trion and exciton decay constants. This implies that the intermediate state is not a real state but an artifact related to the finite time resolution of our experiment, resulting in the mixing of exciton and trion emissions. This is also confirmed again by the curvature of the FLID in Figure 1h. During a unity bin time T, a single QD stays in State 1 (intensity I_1, lifetime τ_1) for time T_1, and in State 2 (intensity I_2, lifetime τ_2) for time T_2. Then the average intensity I and the average lifetime τ for the whole bin time *T* are

$$T = T_1 + T_2,$$

$$I = \frac{I_1 T_1 + I_2 T_2}{T},$$
$$\tau = \frac{I_1 T_1 \tau_1 + I_2 T_2 \tau_2}{I_1 T_1 + I_2 T_2}.$$

Then the average lifetime τ is inversely proportional to the average intensity I as

$$\tau = \frac{I_1 I_2 (\tau_2 - \tau_1)}{I_1 - I_2} \frac{1}{I} + \frac{I_1 \tau_1 - I_2 \tau_2}{I_1 - I_2} \qquad (2).$$

This is very different to Equation (1). Inputting the known PL lifetimes and intensities of both the exciton and trion states, the curvature in the FLID plot, is reproduced by Equation (2) (the white line in Figure 1h). Importantly, surface traps play an important role in both Auger-blinking and in BC-blinking. Adsorbate mobility, surface diffusion and desorption events, generate short-lived traps (*e.g.*, shallow traps) which lead to nonradiative-rate fluctuations and hence BC-blinking, while for the formation of the trion long-lived traps are required (*e.g.*, deep traps). Once a carrier from the first exciton is trapped, it must be relatively long-lived so that there is enough time to generate a second exciton to form a trion.

C. The coexistence of the two blinking mechanisms

Pure BC-blinking or pure Auger- (exciton-trion) blinking occurs rarely. In most cases, both mechanisms coexist and a mixture of blinking behaviors are observed. This coexistence is illustrated by two typical single QDs, QD 3 and QD 4 in Figure 2 (both are QD@639nm). The emission of QD 3 jumps among a set of levels, and the trion emission level is blurred. Conversely, for QD 4, the trion state is located at an intensity level of 180 counts / 20 ms. Despite a slightly bending in the FLID of QD 4, both FLIDs are basically linear (Figures 2b and

2e). As mentioned above, this linear correlation between the intensity and lifetime is a signature of BC-blinking. In order to see the trion state feature clearly, the FLIDs are presented as scatter plots in Figures 2b and 2e rather than color maps used in Figure 1. In the lower left corner of both FLIDs, there is a small feature above the main linear pattern indicated by red triangles in Figure 2b and 2e, which is a signature of the trion state. We can compute the radiative lifetime scaling. The brightest exciton state is selected for computation. In principle, any part of the linear pattern of FLID can be used because they all are from excitons but each part of the distribution corresponds to a period with different non-radiative decay rates. The single-exponential PL decays of the brightest exciton state and of the trion states are plotted in Figures 2c and 2f. Again the radiative lifetime scaling order is around 2.

$$\frac{\tau_{Xr}}{\tau_{X^*r}} = \frac{\tau_X}{\tau_{X^*}} \cdot \frac{I_{X^*}}{I_X} = \frac{24.2}{4.4} \times \frac{218-2}{600-2} \approx 1.99 \text{ for QD 3;}$$
$$\frac{\tau_{Xr}}{\tau_{X^*r}} = \frac{\tau_X}{\tau_{X^*}} \cdot \frac{I_{X^*}}{I_X} == \frac{33.3}{4.5} \times \frac{180-2}{670-2} \approx 1.97 \text{ for QD 4.}$$

From the above experiments, it is evident that there are two coexisting mechanisms of PL intermittency: BC-blinking and Auger-blinking. These two types of blinking can also be found in the other batch of QDs (QD@618nm) with a smaller core size. The environmental experiments on QD@618nm reveal that both types of blinking, especially BC-blinking, are highly influenced by the surface condition of QDs (see Supplementary Information).

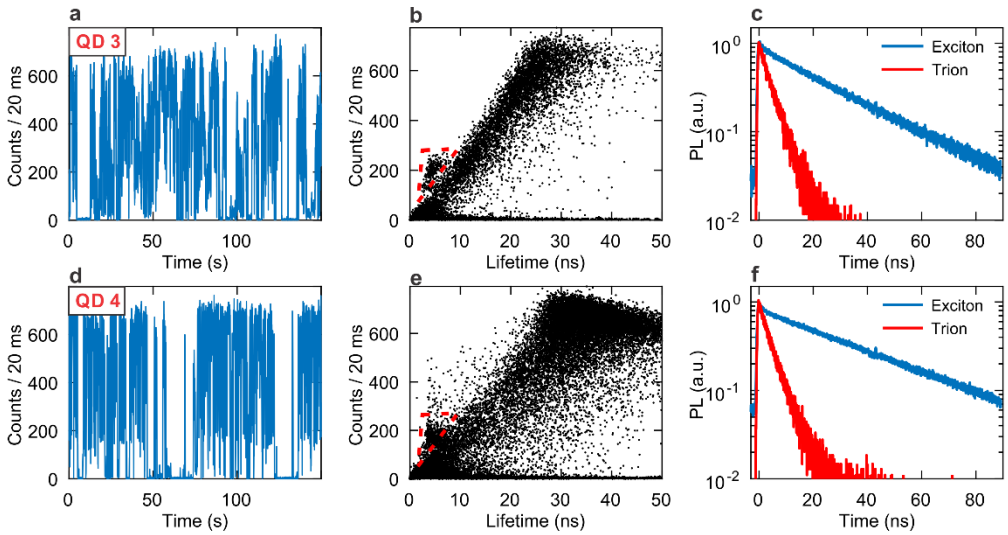

Figure 2 **The coexistence of BC-blinking and Auger-blinking.** Two single QDs (QD@639 nm) were excited at 400 nW. QD 3 (the top three panels) and QD 4 (the bottom three panels). **(a,d)** Photoluminescence intensity traces: (a) QD 3 - multiple intensity levels appear but there is no clear trion level; (d) QD 4 - trion emission is discernible. **(b,e)** The FLIDs of (b) QD 3 and (e) QD 4. Trions are labelled with red triangles. **(c,f)** Exciton (blue line) and trion (red line) decays of (c) QD 3 and (f) QD 4.

D. Exponential and power-law Auger-blinking

The blinking statistics for a single QD can be quasi-exponential or exponential. For example, the exciton-trion blinking of QD 2 is shown again in Figure 3a. The PL intensity is divided from low to high into four parts: dark, trion, mixed, and exciton states in Figure 3b. The histograms of exciton and trion state durations are described by an exponential distribution and not by a power law in Figure 3c and 3d. Similar exponential distributions have been reported previously.[15] The exponential behavior implies that the charging and discharging rates do not change much with time. Multiple traps with varying barriers are used to explain the power-law blinking.[9] The exponential blinking indicates that the distribution of trap barriers is narrow in QD 3. In comparison, a different single QD with a smaller core size, QD 5, from the other batch of QDs (QD@618nm) shows different exciton-trion blinking. While the same exponential distribution is observed for the trion state duration in Figure 3h, the exciton state duration is power-law

governed in Figure 3g. The QD 5 switches rapidly between the neutral and charged states in the first 25 s. The blinking rate is substantially reduced in the following 25 s (Figure 3e). This implies that the trapping channel can be blocked and unblocked during Auger-blinking as well as in the BC-blinking. This can explain why the neutral exciton state of QD 5 obeys a power law. The fast and slow charging here can also be well fitted using a biexponential function with two charging rates (Supplementary Figure 2).

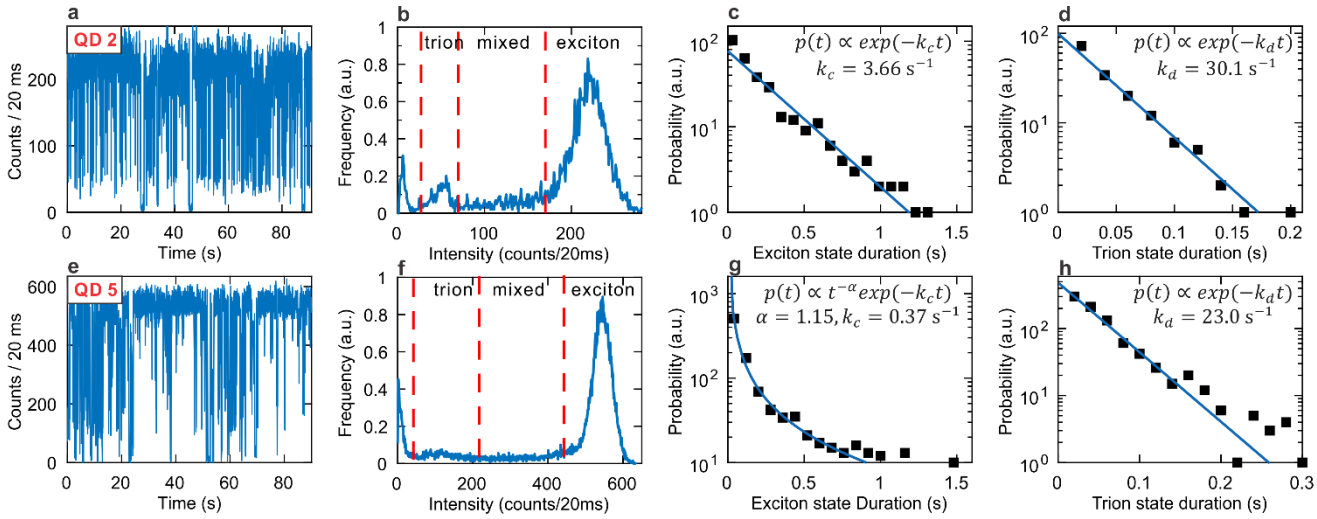

Figure 3 **Exponential and power-law Auger-blinking.** The top four panels are the exponential blinking from QD 2 (QD@639nm) excited at 100 nW. The bottom four panels are the power-law blinking from QD 5 (a different batch, QD@618nm) excited at 200 nW. Bin size is 20 ms. **(a,e)** Photoluminescence intensity traces: (a) QD 2 and (e) QD 5. **(b,f)** Histograms of the measured intensity: (b) QD 2 and (f) QD 5. The red dash lines divide the intensity from low to high into four parts: dark state, trion state, mixed state, and exciton state. **(c,g)** Statistics of exciton state duration (black squares) in semilogarithmic scale: (c) QD 2 and (g) QD 5. The distributions are fitted by a single exponential function and a truncated power-law function (blue line), respectively. **(d,h)** Statistics of trion state duration (black squares) in semilogarithmic scale: (d) QD 2 and (h) QD 5. Both distributions are fitted by single exponential functions (blue line).

For the BC-blinking with a continuous distribution of emission states, we are not able to analyze the statistics of duration, because it is not proper anymore to use a threshold line to divide on

and off states. Since the BC-blinking always exists, it may distort the experimental duration histograms of exciton and trion states.

E. The effect of excitation power on exponential Auger-blinking

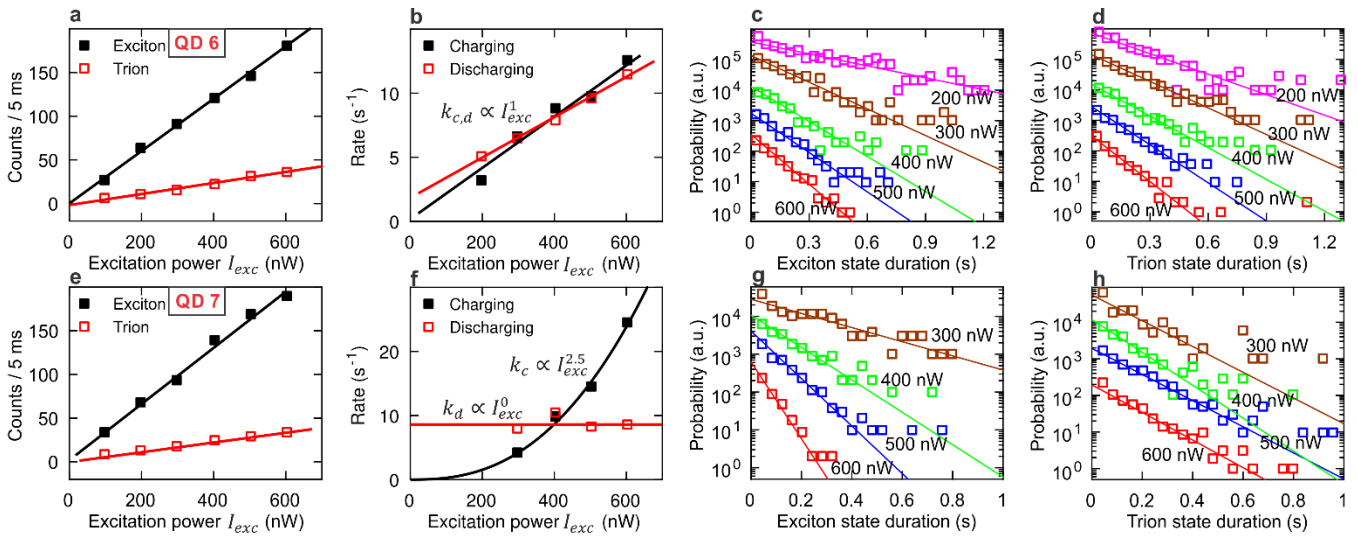

Figure 4 **The effect excitation power on exponential Auger-blinking.** QD 6 (top four panels) and QD 7 (bottom four panels) are from QD@639nm. **(a,e)** The linear dependence of exciton (black solid square) and trion (red open square) intensities on excitation power: (a) QD 6 and (e) QD 7. **(b,f)** The dependence of charging (black solid square) and discharging (red open square) rates on excitation power: (b) QD 6 and (f) QD 7. The charging and discharging rates are extracted from (c),(d),(g) and (h) with the 95% confidence bounds smaller than the marker size. **(c,g)** The exponential distributions of exciton state duration: (c) QD 6 and (g) QD 7. **(d,h)** The exponential distributions of trion state duration: (d) QD 6 and (h) QD 7. Each distribution is labeled with excitation power.

The effects of excitation power on the exponential charging-blinking for two single QDs is presented in Figure 4 and in Supplementary Figures 8 and 9. The intensities of both the exciton and trion states are plotted as a function of excitation power in Figures 4a and 4e, and the rates of charging and discharging are plotted in Figures 4b and 4f. The charging rate, k_c, and discharging rate, k_d, are extracted from the exponential histograms of exciton and trion state

durations at different excitation powers in Figures 4c, 4d, 4g and 4h.The duration distributions of exciton and trion states, $P(t)$, are dependent on k_c and k_d as

$$P(t) \propto exp(-k_{c\ or\ d}t).$$

Many reports have studied the dependence of the ionization rate on the power.[35, 43-49] It has been postulated that hot carriers from Auger recombination of biexcitons may contribute to the ionization events, and that the excitation power dependence under low excitation conditions is quadratic.[5, 43-45] However, a linear dependence has also been reported, and this indicates that traps can capture carriers directly from single excitons.[48-50] Here, we observe a linear dependence of the charging rate on the power for QD 6 (Figure 4b), and a quasi-quadratic dependence for QD 7 (Figure 4f). As the excitation power increases, the emission intensities of exciton and trion states increase linearly without saturation (Figure 4a and 4e). This demonstrates that the QDs are still in the low excitation regime. In Figure 4b, the charging rate increases linearly with the excitation power and a zero intercept is inferred. The zero intercept of the charging rate is reasonable because it is impossible to photocharge QDs without light. For QD 7, a zero intercept of the charging rate can also be obtained using a quasi-quadratic function.

The discharging rate characterizes how fast a QD transitions from the trion state to the neutral state. We do not know whether it is a positive or negative trion here, but we take a negative trion for example. The significant, nonzero intercept of the discharging rate in Figures 4b and 4f means that the trapped hole at the surface can return spontaneously to the negatively charged

core in the dark, making the core neutral.[49] For QD 7, the discharging rate does not rely too much on the excitation power, which means that only spontaneous neutralization exists. For QD 8, however, the discharging process is assisted by the light.[15, 49] Under illumination, the negative trion will be formed when a second exciton is generated in a negatively charged core. If the hole of the negative trion is captured by surface traps and two electrons are left in the core, then the QD core is doubly charged. This will convert the QD from the normal grey state into a much less emissive dim or even dark state. One electron of the negative trion can accept the energy from the Auger recombination and overcome the barrier. Once this hot electron reaches the surface traps or recombines with the surface trapped hole, the QD core becomes neutral. Both multiple charging and neutralization are possible. However, multiple charging events can be neglected, because we have shown that the majority of PL jumps occur between bright (exciton) and grey (trion) states (see the blinking traces in Supplementary Figures 8 and 9).

Summary

We have shown experimentally that two types of PL blinking can exist in the same single QD: the first is due to fluctuations in the non-radiative recombination rate alone, while the second type involves both radiative and non-radiative rate-jumps due to charging. The two kinds of blinking are depicted graphically in Figure 5. In BC-blinking, the non-radiative rate fluctuates because of the activation and deactivation of short-lived surface traps. Competition occurs between the fixed radiative and fluctuating non-radiative decay rates for band-edge excitons. This leads to a linear correlation between the PL lifetime and the PL intensity; this is quite distinct from HC-blinking where the PL lifetime is constant. In Auger-blinking, both radiative and non-radiative rates change when the QD switches between the neutral and charged states. The

Auger-blinking is also affected by opening and closing of the trapping channel, leading to a conventional power-law distributed *on* and *off* durations. However, if the traps are always active, the blinking exhibits a quasi-exponential distribution. We propose further that BC- blinking is due to fast trapping and then non-radiative recombination *via* short-lived traps, while long-lived traps are involved in the exciton-trion transition.

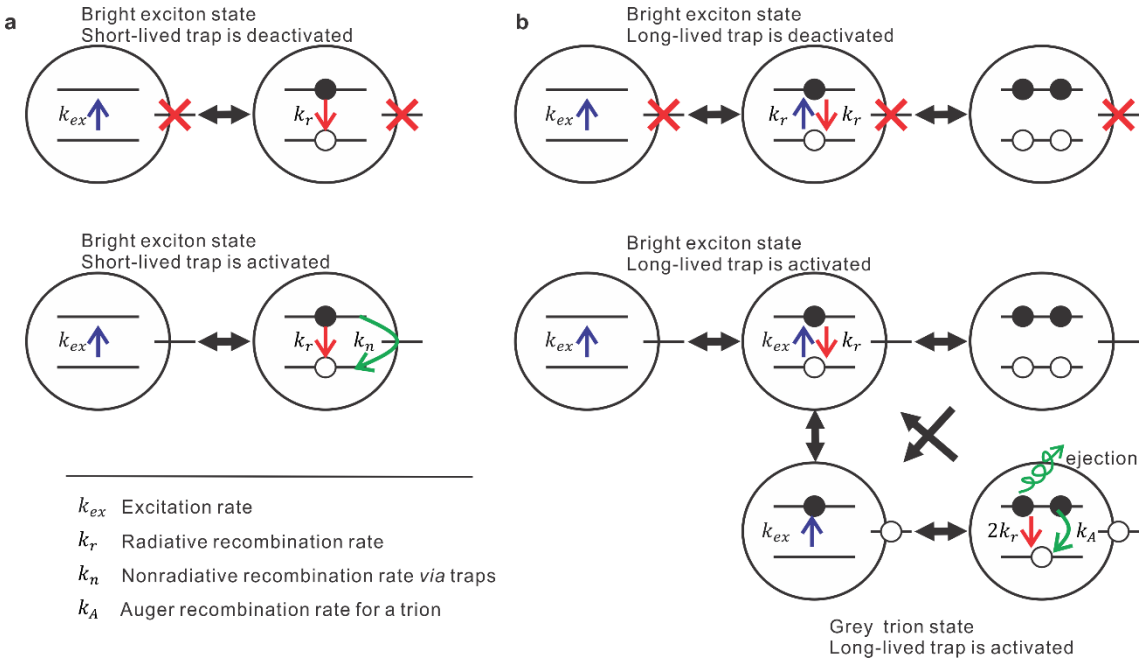

Figure 5 **Simplified kinetics of blinking.** (a) BC-blinking. When traps are deactivated, the QD is in bright state with the zero non-radiative rate; when traps are activated, in addition to the radiative decay, the exciton can also non-radiatively decay via traps. (b) Auger-blinking (exciton-trion blinking). In the first row, the traps are deactivated and the QD is in the bright state. In the second row, the long-lived traps are activated but no electron is trapped due to the slow trapping rate. In the third row, a hole is trapped due to exciton ionization and biexciton ionization. The core is negatively charged. Because of the long-lived trapped hole, the second exciton is generated by further excitation, and then the non-radiative Auger decay competes with the radiative decay. The charging state can be neutral again via spontaneous detrapping of the trapped hole or ejecting an electron from core to the surface.

Methods

$CdSe/Cd_xZn_{1-x}S$ QD Synthesis

The QDs were synthesized by following our alloyed shelling method (Ref. 39). Two batches of QDs were used in this work. The synthesis of the small QDs (QD@618 nm, fluorescence peak at 618 nm) started from CdSe cores with a diameter of 4.2 nm and these were overcoated with two shells of nominally 4 monolayer (ML) of CdS and 2 ML of ZnS; the synthesis of the large QDs (QD@618 nm, fluorescence peak at 639 nm) started from 5.4 nm diameter CdSe cores with shells of nominally 4 ML of CdS and 2 ML of ZnS.

QD Measurement

A small drop of dilute QD hexane solution was cast on coverslips. Single NCs were distributed sparsely after spincoating. These single QDs were then overcoated with a 100nm-thick PMMA film by spincoating. Then the coverslips were left in air for measurement.

A custom-built confocal microscope based on Olympus IX71 was used to do single QD measurement. 466 nm pulsed laser diode (PicoQuant, LDH-P-C-470, tunable repetition rate from 2.5 MHz to 20 MHz) was used to excite QDs. The emission was collected through an oil-immersion objective (Olympus, PlanApo NA 1.4), and detected by avalanche photodiodes (Perkin-Elmer, SPCM-AQR-14). The PL trace and decay measurements were carried out with a time-correlated single photon counting (TCSPC) card (PicoQuant, TimeHarp 200) in time-tagged time-resolved mode (TTTR).

Acknowledgements

K. B. acknowledges support from the Humboldt Foundation through a Feodor Lynen-Fellowship (2012-2015) and from the Fonds der Chemischen Industrie (FCI) through a Liebig Fellowship (since 2015). PM thanks the ARC for support through DP130102134 and CE170100026.

Author contributions

G.Y. performed all the spectroscopic work and carried out the data analysis. D.G. helped build the instrumentation and assisted with data analysis. P.M. conceived the experiments and directed the research, K.B. and N.K. designed and synthesized the quantum dots used in the experiments. All the authors contributed to the writing and editing of the final manuscript.

Competing financial interests

The authors declare no competing financial interests.

References

1. Dai X., Deng Y., Peng X. & Jin Y. Quantum-Dot Light-Emitting Diodes for Large-Area Displays: Towards the Dawn of Commercialization. *Adv. Mater.* **29,** 1607022-n/a (2017).

2. Aharonovich I., Englund D. & Toth M. Solid-state single-photon emitters. *Nature Photonics* **10,** 631-641 (2016).

3. Nirmal M.*, et al.* Fluorescence intermittency in single cadmium selenide nanocrystals. *Nature* **383,** 802-804 (1996).

4. Efros A. L. & Nesbitt D. J. Origin and control of blinking in quantum dots. *Nature Nanotech.* **11,** 661-671 (2016).

5. Efros A. L. & Rosen M. Random telegraph signal in the photoluminescence intensity of a single quantum dot. *Phys. Rev. Lett.* **78,** 1110 (1997).

6. Krauss T. D. & Brus L. E. Charge, Polarizability, and Photoionization of Single Semiconductor Nanocrystals. *Phys. Rev. Lett.* **83,** 4840-4843 (1999).

7. Kuno M., Fromm D., Hamann H., Gallagher A. & Nesbitt D. Nonexponential "blinking" kinetics of single CdSe quantum dots: A universal power law behavior. *J. Chem. Phys.* **112,** 3117-3120 (2000).

8. Verberk R., van Oijen A. M. & Orrit M. Simple model for the power-law blinking of single semiconductor nanocrystals. *Phys. Rev. B* **66,** (2002).

9. Kuno M., Fromm D. P., Johnson S. T., Gallagher A. & Nesbitt D. J. Modeling distributed kinetics in isolated semiconductor quantum dots. *Phys. Rev. B* **67,** (2003).

10. Tang J. & Marcus R. A. Diffusion-controlled electron transfer processes and power-law statistics of fluorescence intermittency of nanoparticles. *Phys. Rev. Lett.* **95,** 107401 (2005).

11. Pelton M., Smith G., Scherer N. F. & Marcus R. A. Evidence for a diffusion-controlled mechanism for fluorescence blinking of colloidal quantum dots. *Proc. Natl. Acad. Sci. USA* **104,** 14249-14254 (2007).

12. Zhao J., Nair G., Fisher B. R. & Bawendi M. G. Challenge to the charging model of semiconductor-nanocrystal fluorescence intermittency from off-state quantum yields and multiexciton blinking. *Phys. Rev. Lett.* **104,** 157403 (2010).

13. Rosen S., Schwartz O. & Oron D. Transient fluorescence of the off state in blinking CdSe/CdS/ZnS semiconductor nanocrystals is not governed by Auger recombination. *Phys. Rev. Lett.* **104,** (2010).

14. Jha P. P. & Guyot-Sionnest P. Trion decay in colloidal quantum dots. *ACS Nano* **3,** 1011-1015 (2009).

15. Gomez D. E., van Embden J., Mulvaney P., Fernee M. J. & Rubinsztein-Dunlop H. Exciton-trion transitions in single CdSe-CdS core-shell nanocrystals. *ACS Nano* **3,** 2281-2287 (2009).

16. Spinicelli P.*, et al.* Bright and grey states in CdSe-CdS nanocrystals exhibiting strongly reduced blinking. *Phys. Rev. Lett.* **102,** (2009).

17. Zhang K., Chang H., Fu A., Alivisatos A. P. & Yang H. Continuous distribution of emission states from single CdSe/ZnS quantum dots. *Nano Lett.* **6,** 843-847 (2006).

18. Fisher B. R., Eisler H.-J., Stott N. E. & Bawendi M. G. Emission intensity dependence and single-exponential behavior in single colloidal quantum dot fluorescence lifetimes. *J. Phys. Chem. B* **108,** 143-148 (2004).

19. Schmidt R., Krasselt C., Göhler C. & von Borczyskowski C. The fluorescence intermittency for quantum dots is not power-law distributed: a luminescence intensity resolved approach. *ACS Nano* **8,** 3506-3521 (2014).

20. Schlegel G., Bohnenberger J., Potapova I. & Mews A. Fluorescence decay time of single semiconductor nanocrystals. *Phys. Rev. Lett.* **88,** (2002).

21. Frantsuzov P. A. & Marcus R. A. Explanation of quantum dot blinking without the long-lived trap hypothesis. *Phys. Rev. B* **72,** (2005).

22. Frantsuzov P., Volkán-Kacsó S. & Jankó B. Model of fluorescence intermittency of single colloidal semiconductor quantum dots using multiple recombination centers. *Phys. Rev. Lett.* **103,** (2009).

23. Rabouw F. T.*, et al.* Delayed exciton emission and its relation to blinking in CdSe quantum dots. *Nano Lett.* **15,** 7718-7725 (2015).

24. Sampat S.*, et al.* Multistate blinking and scaling of recombination rates in individual Silica-coated CdSe/CdS nanocrystals. *ACS Photonics* **2,** 1505-1512 (2015).

25. Javaux C.*, et al.* Thermal activation of non-radiative Auger recombination in charged colloidal nanocrystals. *Nature Nanotech.* **8,** 206-212 (2013).

26. Kambhampati P. Hot exciton relaxation dynamics in semiconductor quantum dots: radiationless transitions on the nanoscale. *J. Phys. Chem. C* **115,** 22089-22109 (2011).

27. Galland C.*, et al.* Lifetime blinking in nonblinking nanocrystal quantum dots. *Nat. Commum.* **3,** 908 (2012).

28. Qin W. & Guyot-Sionnest P. Evidence for the role of holes in blinking: negative and oxidized CdSe/CdS dots. *ACS Nano* **6,** 9125-9132 (2012).

29. Galland C.*, et al.* Two types of luminescence blinking revealed by spectroelectrochemistry of single quantum dots. *Nature* **479,** 203-207 (2011).

30. Cragg G. E. & Efros A. L. Suppression of auger processes in confined structures. *Nano Lett.* **10,** 313-317 (2010).

31. Chen Y.*, et al.* "Giant" multishell CdSe nanocrystal quantum dots with suppressed blinking. *J. Am. Chem. Soc.* **130,** 5026-5027 (2008).

32. Omogo B., Gao F., Bajwa P., Kaneko M. & Heyes C. D. Reducing blinking in small core-multishell quantum dots by

carefully balancing confinement potential and induced lattice strain: the "Goldilocks" effect. *ACS Nano* **10,** 4072-4082 (2016).

33. Chen O.*, et al.* Compact high-quality CdSe-CdS core-shell nanocrystals with narrow emission linewidths and suppressed blinking. *Nature Mater.* **12,** 445-451 (2013).

34. Mahler B.*, et al.* Towards non-blinking colloidal quantum dots. *Nature Mater.* **7,** 659-664 (2008).

35. Qin H.*, et al.* Single-dot spectroscopy of zinc-blende CdSe/CdS core/shell nanocrystals: nonblinking and correlation with ensemble measurements. *J. Am. Chem. Soc.* **136,** 179-187 (2014).

36. Stefani F. D., Hoogenboom J. P. & Barkai E. Beyond quantum jumps: blinking nanoscale light emitters. *Phys. Today* **62,** 34-39 (2009).

37. Frantsuzov P., Kuno M., Janko B. & Marcus R. A. Universal emission intermittency in quantum dots, nanorods and nanowires. *Nature Phys.* **4,** 519-522 (2008).

38. Cordones A. A. & Leone S. R. Mechanisms for charge trapping in single semiconductor nanocrystals probed by fluorescence blinking. *Chem. Soc. Rev.* **42,** 3209-3221 (2013).

39. Osad'ko I. S., Eremchev I. Y. & Naumov A. V. Two mechanisms of fluorescence intermittency in single core/shell quantum dot. *J. Phys. Chem. C* **119,** 22646-22652 (2015).

40. Boldt K., Kirkwood N., Beane G. A. & Mulvaney P. Synthesis of highly luminescent and photo-stable, graded shell CdSe/CdxZn1–xS nanoparticles by in situ alloying. *Chem. Mater.* **25,** 4731-4738 (2013).

41. Voznyy O. Mobile surface traps in CdSe nanocrystals with carboxylic acid ligands. *J. Phys. Chem. C* **115,** 15927-15932 (2011).

42. Houtepen A. J., Hens Z., Owen J. S. & Infante I. On the origin of surface traps in colloidal II–VI semiconductor nanocrystals. *Chem. Mater.* **29,** 752-761 (2017).

43. Eremchev I. Y., Osad'ko I. S. & Naumov A. V. Auger ionization and tunneling neutralization of single CdSe/ZnS nanocrystals revealed by excitation intensity variation. *J. Phys. Chem. C* **120,** 22004-22011 (2016).

44. Cordones A. A., Bixby T. J. & Leone S. R. Evidence for multiple trapping mechanisms in single CdSe/ZnS quantum dots from fluorescence intermittency measurements over a wide range of excitation intensities. *J. Phys. Chem. C* **115,** 6341-6349 (2011).

45. Peterson J. J. & Nesbitt D. J. Modified power law behavior in quantum dot blinking: a novel role for biexcitons and auger ionization. *Nano Lett.* **9,** 338-345 (2008).

46. Bruhn B., Qejvanaj F., Sychugov I. & Linnros J. Blinking statistics and excitation-dependent luminescence yield in Si and CdSe nanocrystals. *J. Phys. Chem. C* **118,** 2202-2208 (2014).

47. Knappenberger K. L., Wong D. B., Romanyuk Y. E. & Leone S. R. Excitation wavelength dependence of fluorescence intermittency in CdSe/ZnS core/shell quantum dots. *Nano Lett.* **7,** 3869-3874 (2007).

48. Stefani F., Knoll W., Kreiter M., Zhong X. & Han M. Quantification of photoinduced and spontaneous quantum-dot luminescence blinking. *Phys. Rev. B* **72,** (2005).

49. Meng R.*, et al.* Charging and discharging channels in photoluminescence intermittency of single colloidal CdSe/CdS Core/Shell quantum dot. *J. Phys. Chem. Lett.* **7,** 5176-5182 (2016).

50. Banin U.*, et al.* Evidence for a thermal contribution to emission intermittency in single CdSe/CdS core/shell nanocrystals. *J. Chem. Phys.* **110,** 1195-1201 (1999).

Supplementary Information

Two Mechanisms Determine Quantum Dot Blinking

Gangcheng Yuan[1], Daniel E. Gomez[2], Nicholas Kirkwood[1,3], Klaus Boldt[1,4], and Paul Mulvaney[1]*

1 School of Chemistry and Bio21 Institute, University of Melbourne, Parkville, Victoria 3010, Australia
2 RMIT University, Melbourne, Victoria, 3000, Australia.

3 Current Address: Opto-Electronic Materials Section, Faculty of Applied Sciences, Delft University of Technology, Van der Maasweg 9, 2629HZ Delft, The Netherlands
4 Current Address:Department of Chemistry and Zukunftskolleg, University of Konstanz, 78457 Konstanz, Germany
** e-mail: mulvaney@unimelb.edu.au*

A. BC-blinking for QD@618nm

Supplementary Figure 1a shows a typical PL intensity time trace collected from a single QD (single QD 8, QD@618nm). A low excitation power (50 nW) was used to reduce the ionization rate. To establish a relationship between the lifetime and intensity, the intensity is divided arbitrarily into 7 levels. After fitting each PL decay to a single exponential function, the lifetime is assigned to each level. As indicated in Supplementary Figure 1b, the intensity increases almost linearly as the lifetime increases except in the upper right area (lifetime τ > 20 ns, intensity I > 100 counts / 20 ms). In the right-upper corner, there is a steep rise in the intensity but the lifetime almost remains the same, because these artificially defined levels are from the same bright state. The linear correlation between the lifetime and intensity has also been confirmed by fluorescence lifetime-intensity distributions (FLID) shown in Supplementary Figure 1c. In Supplementary Figure 1d, QD 9 (QD @ 618 nm) can sojourn in some states for a time of up to ten seconds. Three periods with stable PL intensities, presented in Supplementary Figure 1d, 201-211s, 213s-225s and 257s-264s, are selected for the intensity-lifetime analysis, outlined below. Within each period, the intensity is stable (I_1=37 counts / 20 ms, I_2=97 counts / 20 ms, and I_3=16 counts / 20 ms), and the PL decays in Supplementary Figure 1e can be fitted well using a single exponential function (τ_1=33 ns, τ_2=12 ns, and τ_3=4.9 ns). The radiative lifetime ratio of the three periods is close to unity as

$$\tau_{r1}:\tau_{r2}:\tau_{r3} = \frac{\tau_1}{I_1}:\frac{\tau_2}{I_2}:\frac{\tau_3}{I_3} = \frac{12}{37-2.5(\text{noise})}:\frac{33}{97-2.5}:\frac{4.9}{16-2.5} \approx 1:1:1\,.$$

Not surprisingly, the FLID of QD 9 also shows a linear pattern, see Supplementary Figure 1f.

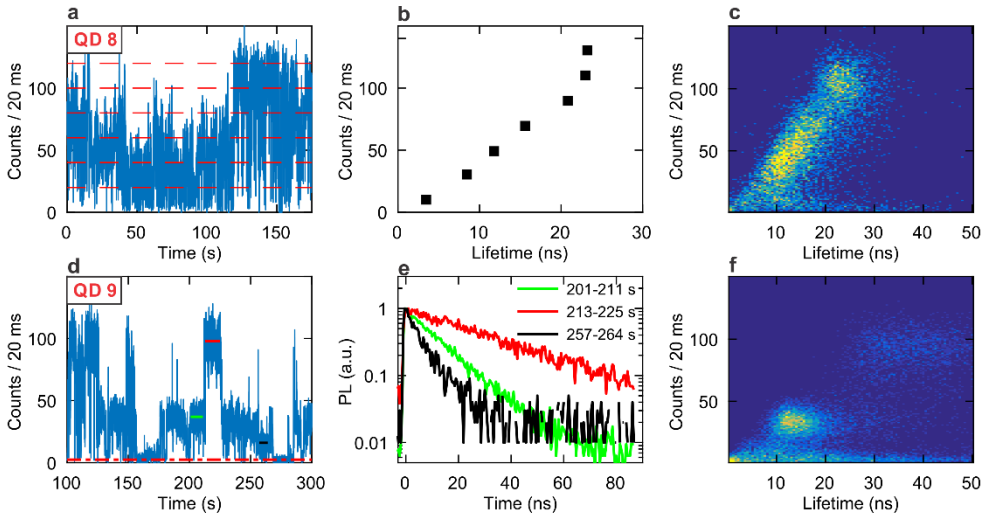

Supplementary Figure 1 - **BC-blinking for QD@618nm.** QD 8 (top three panels) and QD 9 (bottom three panels) were excited at 50 nW. **(a)** Photoluminescence intensity trace of QD 8. The intensity is divided arbitrarily into 7 levels by the red dashed lines. **(b)** The PL Lifetimes of the 7 levels extracted from fits with a single exponential function. **(c)** The FLID of QD 8. **(d)** Photoluminescence intensity trace of QD 9. The background noise (2.5 counts / 20 ms) is indicated by the red dashed line. Three periods, 201-211s (37 counts / 20ms, green marker), 213-225s (97 counts / 20 ms, red marker) and 257s-264s (16 counts / 20 ms, black markers). **(e)** Photoluminescence time decays from the three marked periods, 201-211s (green line), 213-225s (red line) and 257s-264s (black line). Lifetimes are 12ns, 33ns and 4.9ns, respectively. **(f)** The FLID of QD 9.

B. Auger-blinking for QD@618nm

Supplementary Figure 2 shows more about the blinking of QD 5 (QD@618nm) in Figure 3. The ratio of the two radiative lifetimes, τ_{Xr} and τ_{X^*r}, is

$$\frac{\tau_{Xr}}{\tau_{X^*r}} = \frac{\tau_X}{\tau_{X^*}} \cdot \frac{I_{X^*}}{I_X} = \frac{25.2}{2.2} \times \frac{100-2}{545-2} \approx 2.06\,.$$

In Supplementary Figure 2c, the FLID of QD 5 is curved, and can be reproduced by Equation (2). In addition, there is a weak linear pattern indicated by a red dashed line, which is due to BC-blinking.

The distribution of exciton state durations is presented in Supplementary Figures 2d-f. The distribution can be fitted by a conventional truncated power law of the form:

$$p(t) \propto t^{-\alpha} e^{-k_c t},$$

where $\alpha = 1.15$, deviating from 1.5, and the inverse of truncation time, $k_c = 0.371\ \mathrm{s}^{-1}$. The power law blinking can be regarded as arising from a series of exponential blinking processes, i.e.

$$p(t) \propto t^{-\alpha} e^{-k_c t} = \sum_i a_i e^{-k_{ci} t},$$

where k_{ci} is the charging rate, and a_i for the weight of the i_{th} exponential blinking process. Here, the blinking can be explained by just two terms, i.e. by a bi-exponential function

$$p(t) \propto a_1 e^{-k_{c1} t} + a_2 e^{-k_{c2} t},$$

The charging rate switches between $k_{c1} = 15.0\ \mathrm{s}^{-1}$ and $k_{c2} = 1.09\ \mathrm{s}^{-1}$. This is consistent with the blinking trace in Supplementary Figure 2a. QD 5 switches rapidly between the neutral and charged states in the first 25 s. Then the blinking rate is reduced in the following 25 s.

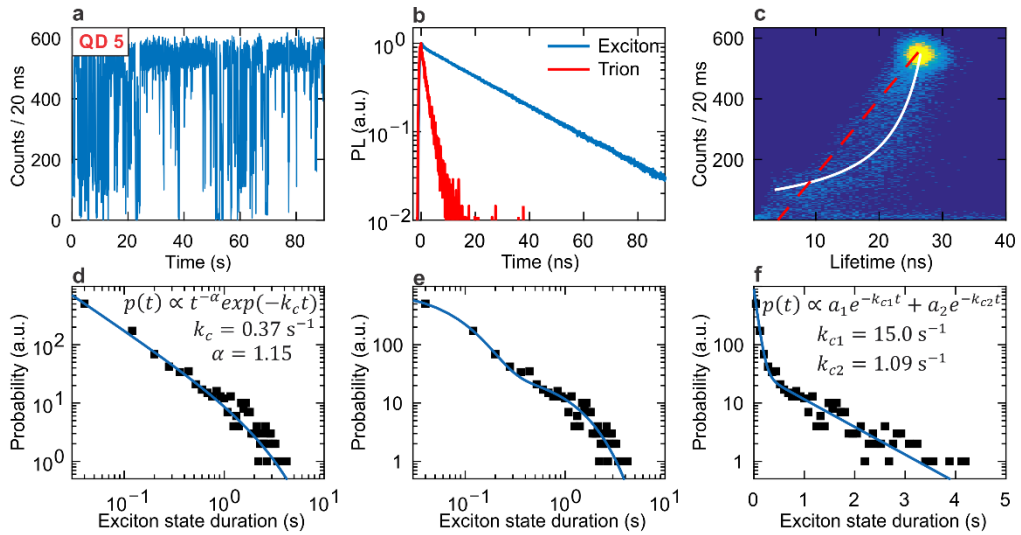

Supplementary Figure 2 - Auger-blinking for QD 5 (QD @618nm) in Figure 3. QD 5 was excited at 200 nW. Bin size is 20 ms. **(a)** Photoluminescence intensity trace. The background is 2 counts / 20 ms. **(b)** Photoluminescence time decays for two intensity levels, exciton (545 counts /20 ms, blue line), trion (100 counts / 20 ms, red line). Both can be fitted by single exponential functions. **(c)** FLID. The white line is given by Equation (2), which is from the exciton-trion transition. The red dashed line indicates that there still exists a linear pattern from the BC-blinking. **(d)** Statistics of exciton state duration (black dots) on a log-log scale. The distribution is fitted by a truncated power-law function (blue line). **(e)** Statistics of exciton state duration (black dots) on a log-log scale. The distribution is fitted by a bi-exponential function (blue line). **(f)** Same as (e) but on a semilogarithmic scale.

C. Environmental effects

For the experiments on atmospheric effects, the stock solution of QDs was moved into a nitrogen glovebox and then diluted with hexane in the nitrogen environment. QDs were spincoated on coverslips and sealed in a chamber before taking them out of the glovebox. The chamber was then mounted on a confocal microscope. The gas in the chamber was changed by flushing a new gas for 10 minutes. Wet gas was produced by water bubbling. The water was pretreated by bubbling with N_2 for one hour to remove the dissolved O_2.

The PL of QDs is sensitive to the condition of the QD surface and the environment. In the following, we compare the blinking of QDs under dry N_2 to that under ambient air. In dry N_2, most

QDs on the glass slide exhibit fast or noisy blinking, which is typical of BC-blinking. Once the same sample is exposed to ambient air, the majority of QDs display neat and stable blinking between *on* and *off* states. Two representative traces from single QDs (QD@618nm), QD 10 in N_2 and QD 11 in air are shown in Supplementary Figure 3. The time-integrated QY for a single QD is calculated by

$$\mathrm{QY} = \frac{\langle I \rangle_T}{I_{max}}$$

where $\langle I \rangle_T$ is the average PL intensity for a period T, and I_{max} is the peak intensity (the bright state intensity). In Supplementary Figure 4, we have calculated the average values of the time-integrated QY for 8 QDs in dry N_2 and another 8 QDs in ambient air. Due to the fast blinking, the time-integrated QY in dry N_2 is low. Once the sample is exposed to ambient air, the QDs observed in air can stay in the bright state for most of the time. Therefore, the average QY of QDs in air is much higher than that of QDs in dry N_2.

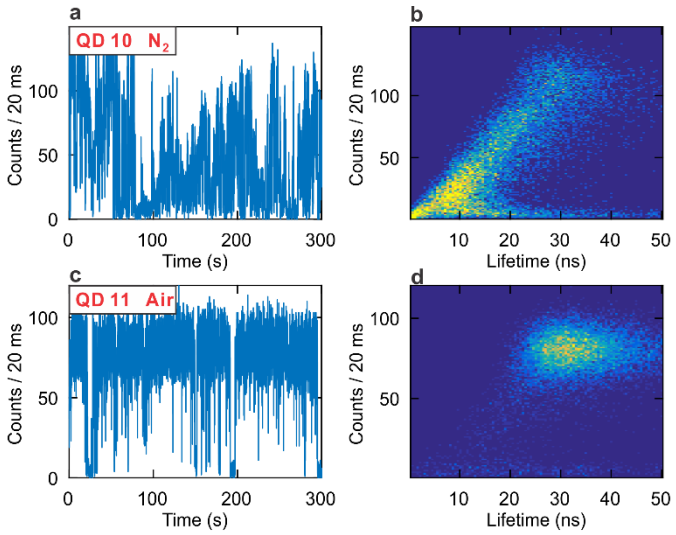

Supplementary Figure 3 - Atmospheric effect on the blinking. Two representative single QDs (QD@618nm) in N_2 and ambient air are shown. The excitation power was 50 nW. Photoluminescence intensity trace of **(a)** QD 10 in N_2, and **(c)** QD 11 in ambient air. FLID of **(b)** QD 10 in N_2, and **(d)** QD 11 in ambient air.

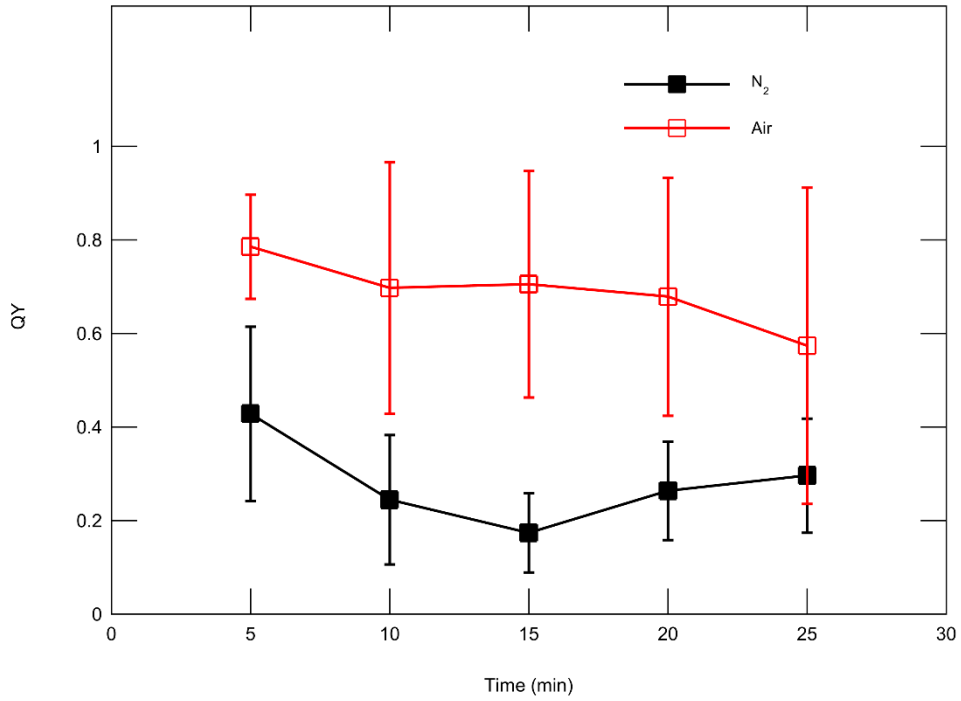

Supplementary Figure 4 - Average time-integrated quantum yields of 8 single QDs in N_2 and another 8 single QDs in ambient air for every 5 min. All single QD@618nm are on the same coverslip, excited at 50 nW.

There are two explanations for the gas-dependent blinking behavior. The first explanation is that O_2 and water in air can suppress blinking by passivating surface states. Although this is partially supported by our finding that O_2 reduces the blinking rate for some QDs (Supplementary Figure 5), most QDs in fact do not respond much to O_2, as shown in Supplementary Figure 6. Supplementary Figure 7 shows the change in PL for the same QDs in dry N_2, wet N_2, dry air and wet air. The moisture can quench the PL of QDs irreversibly. Due to the presence of water vapor, a similar process can be expected in ambient air. We therefore propose an alternative explanation. We assume that the shelling of the majority of QDs is not perfect and that the surface traps are not well passivated. These QDs show fast blinking in N_2 due to these unpassivated traps. In ambient air, a small amount of water is adsorbed onto the unpassivated sites, and the water quenches these QDs. So in air, we only observe neat blinking from well-passivated QDs that are resistant to moisture. No matter which explanation is correct,

the fact is that blinking, especially BC-blinking, is sensitive to the surface condition and environment.

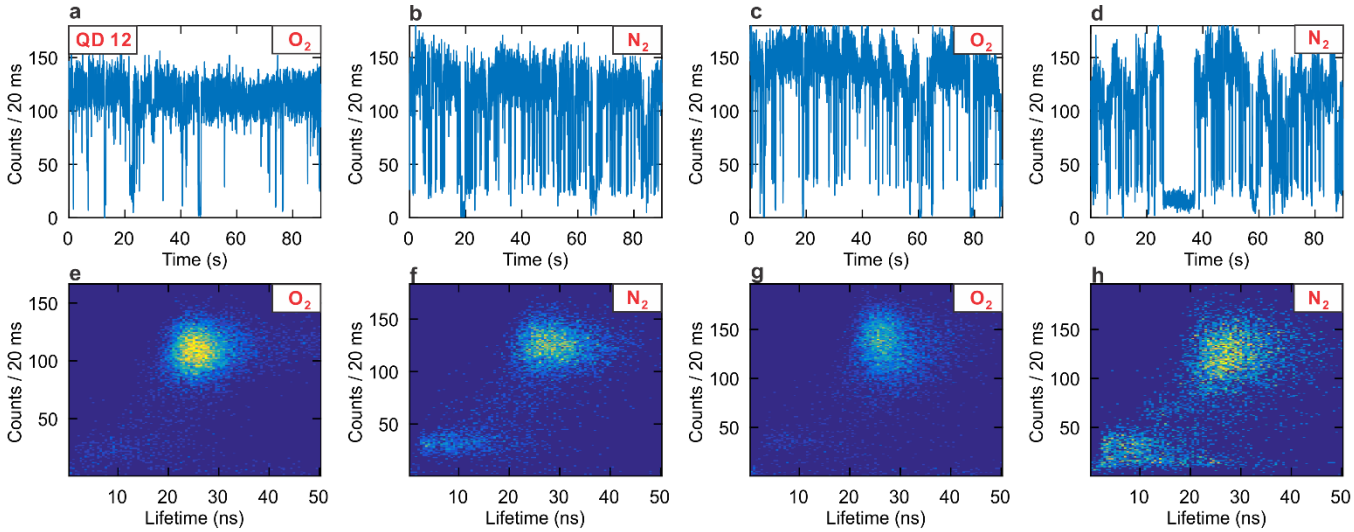

Supplementary Figure 5 - **The blinking behavior of a single QD (QD 12) in dry N_2/O_2.** Photoluminescence intensity traces **(a-d)** and FLIDs **(e-h)** of a single QD, QD@618nm during O_2 and N_2 switching. Although the intensity level of the bright state changes because of objective drift induced by the gas flow, it is still obvious that the blinking rate increases when replacing O_2 with N_2.

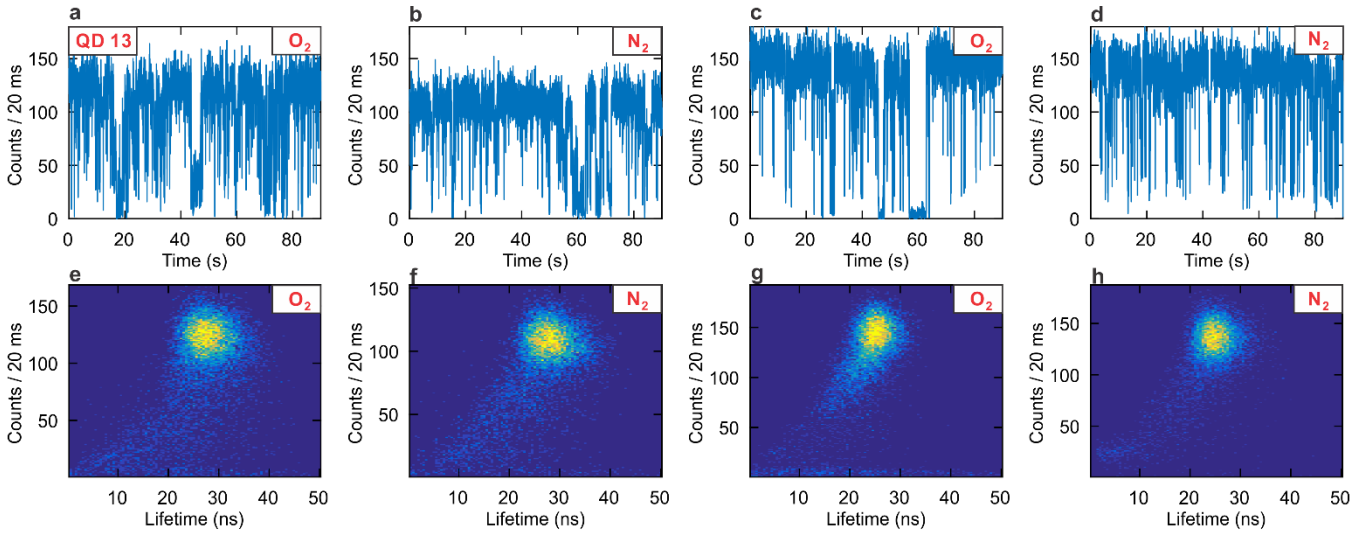

Supplementary Figure 6 - **The blinking behavior of a single QD (QD 13) in dry N_2/O_2.** Photoluminescence intensity traces **(a-d)** and FLIDs **(e-h)** of a single QD @618nm during O_2 and N_2 switching. Apart from small shifts in the intensity level of the bright state due to movement of the microscope objective induced by the gas flow, there is no blinking change as obviously indicated by Supplementary Figure 3.

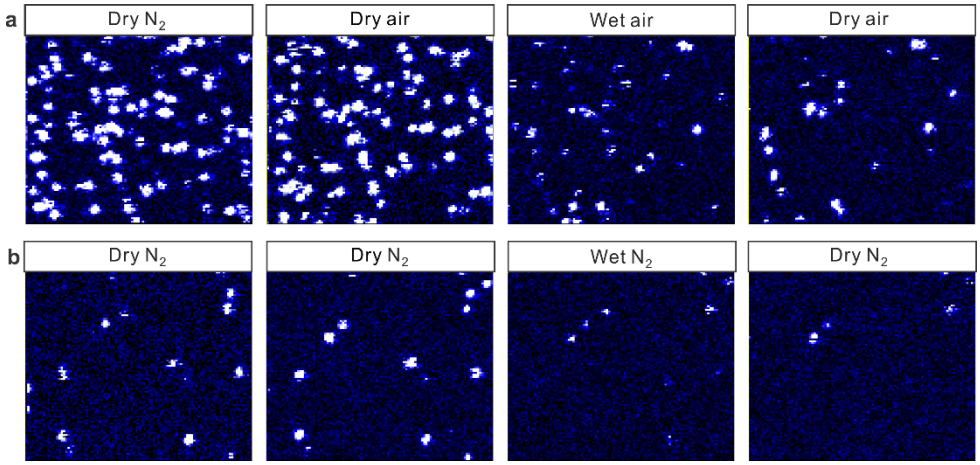

Supplementary Figure 7 - Continuous confocal scanning PL images (10 μm×10 μm) of QDs from QD@618nm. The scanning time of each image is 15 min. The bright spots represent PL from single QDs or clusters. Images in **(a)** recorded sequentially for a region in dry N_2 (from N_2 glovebox), dry air (flushing the chamber with dry air), wet air, and dry air, respectively. Images in **(b)** were recorded sequentially for a region of a new sample in dry N_2 (from N_2 glovebox), dry N_2 (flushing the chamber with dry N_2), wet N_2, and dry N_2, respectively. The gas was changed by flushing the chamber with new gas for 10 min in the dark.

D. Supplementary Information on the effect of excitation power in Figure 4

Since the trion and dark states are very close in intensity in Supplementary Figures 8a and 9a, we cannot use a threshold line to differentiate the dark state and the trion state. Because the majority of PL jumps occur between exciton and trion states (see the blinking trace in Supplementary Figures 8a and 9a), the number of dark state events is negligible. Hence, we only divide the emission from the bottom to the top into three levels: trion, mixed and exciton states. In addition to exciton-trion blinking, there also exists BC-blinking. In general, the intensity levels are continuously distributed and the PL jumps are relatively small for BC-blinking. In order to analyse exactly the duration of exciton and trion states, we can select the periods with sharp jumps. Figure S10 give an example to illustrate how to select the events of exciton and trion for the charging-discharging statistics.

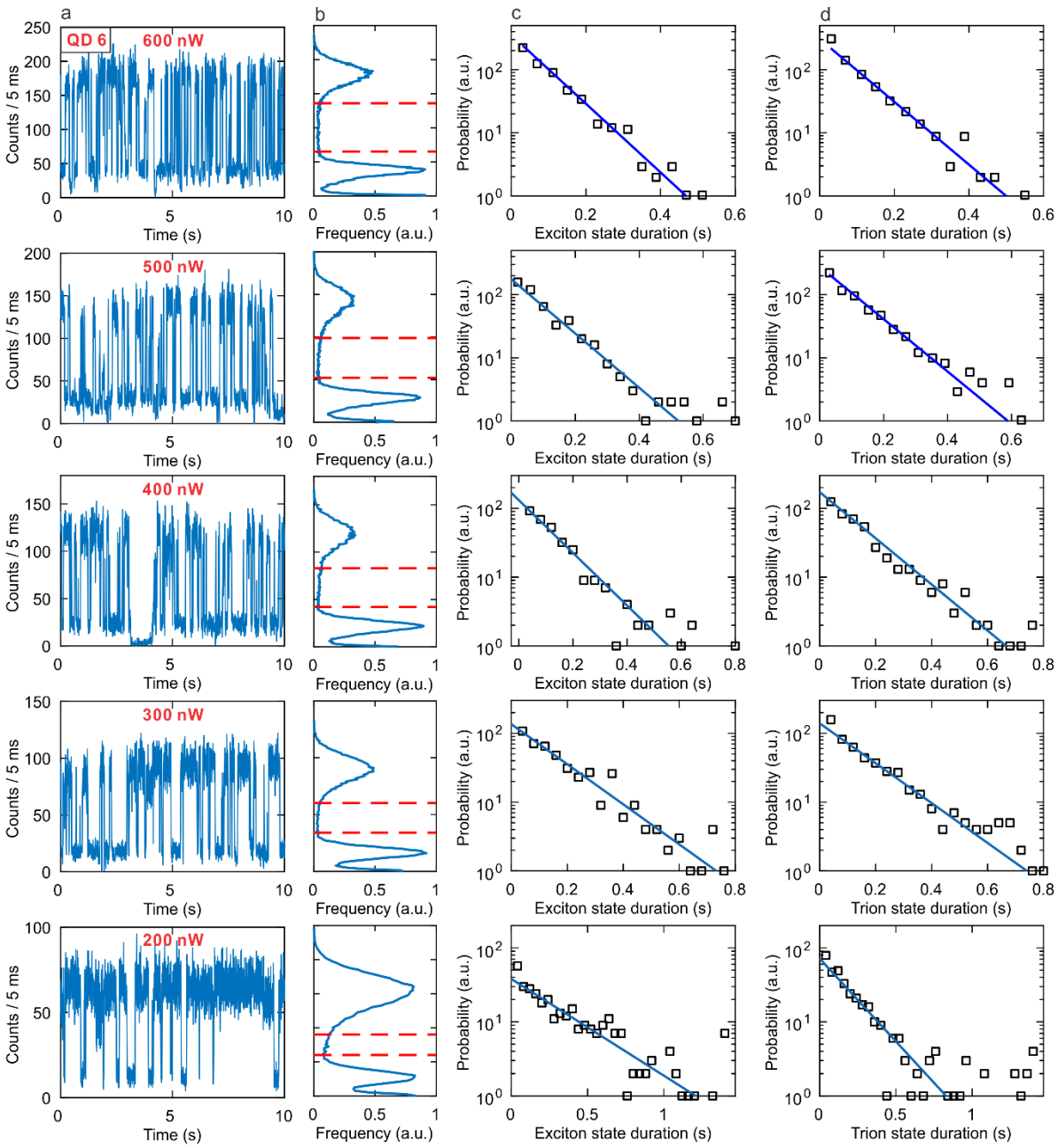

Supplementary Figure 8 - **The excitation power dependence of Auger-blinking for QD 6 in Figure 4**. The excitation power is changed from 600 nW to 200 nW for each row. In columns: **(a)** Photoluminescence intensity trace. **(b)** Histogram of the measured intensity. The red dashed lines divide the intensity from low to high into three characteristic levels attributed to the trion state, mixed state, and exciton state. Statistics of **(c)** exciton state duration and **(d)** trion state duration (black open squares) in semilogarithmic scale. The distributions are fitted by single exponential functions (blue line).

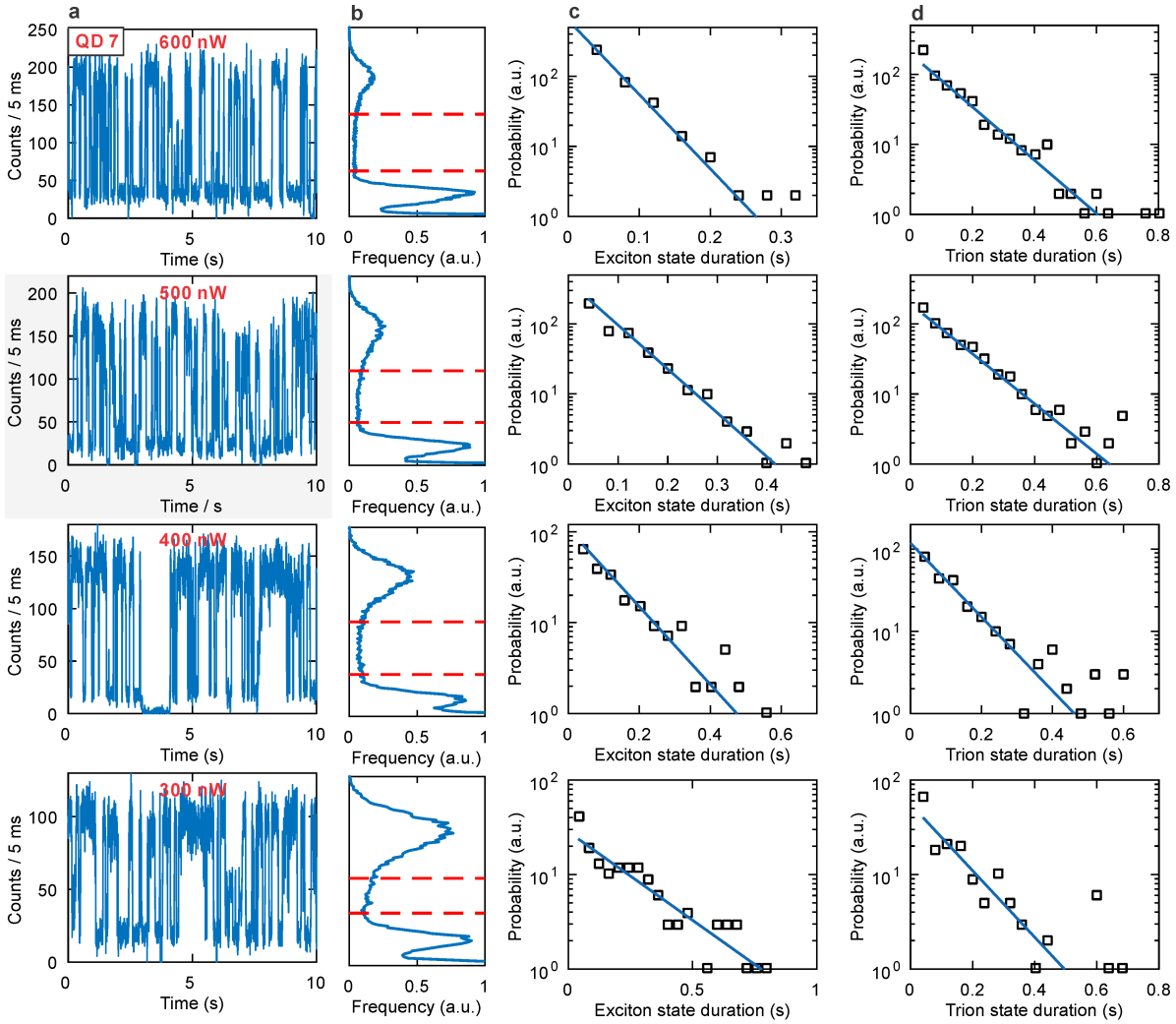

Supplementary Figure 9 - **The excitation power dependence of Auger-blinking for QD 9 in Figure 5.** The excitation power is changed from 600 nW to 300 nW for each row. In columns: **(a)** Photoluminescence intensity trace. **(b)** Histogram of the measured intensity. The red dashed lines divide the intensity from low to high into three characteristic levels attributed to the trion state, mixed state, and exciton state. Statistics of **(c)** exciton state duration and **(d)** trion state duration (black open squares) on a semilogarithmic scale. The distributions are fitted by single exponential functions (blue line).

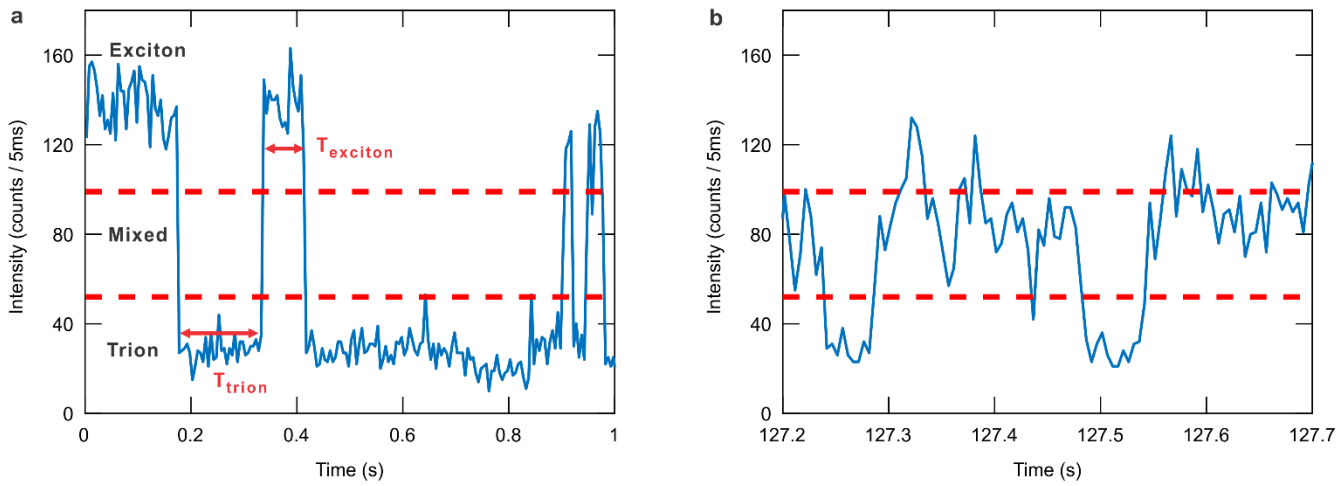

Supplementary Figure 10 - An example of exciton and trion period selection. Exciton and trion states are determined by two threshold lines. The two threshold lines (dash lines) divide the emission into three levels: exciton, mixed states and trion states. Only periods with sharp jumps are selected for duration statistics. **(a)** An exciton period $T_{exciton}$ and an off period T_{trion} are selected as they have sharp jumps between exciton and trion states. **(b)** No periods are selected because there are no sharp jumps. The intensity levels between the two threshold lines arise partly from the BC-blinking.